PROCEEDINGS A

rspa.royalsocietypublishing.org

Research

**Cite this article:** Bardsley OP. 2018 Could hydrodynamic Rossby waves explain the westward drift? *Proc. R. Soc. A* **474**: 20180119. http://dx.doi.org/10.1098/rspa.2018.0119

Received: 19 February 2018
Accepted: 20 April 2018

**Subject Areas:**
geophysics, fluid mechanics, wave motion

**Keywords:**
westward drift, Rossby waves, quasi-geostrophy, Earth's outer core

**Author for correspondence:**
O. P. Bardsley
e-mail: ob275@cam.ac.uk

# Could hydrodynamic Rossby waves explain the westward drift?

O. P. Bardsley

Department of Engineering, University of Cambridge, Trumpington Street, Cambridge CB2 1PZ, UK

OPB, 0000-0002-1525-675X

A novel theory for the origin of the westward drift of the Earth's magnetic field is proposed, based upon the propagation of hydrodynamic Rossby waves in the liquid outer core. These waves have the obscure property that their crests always progress eastwards—but, for a certain subset, energy can nevertheless be transmitted westwards. In fact, this subset corresponds to sheet-like flow structures, extended in both the axial and radial directions, which are likely to be preferentially excited by convective upwellings in the Earth's rapidly rotating outer core. To enable their analysis, the *quasi-geostrophic* (QG) approximation is employed, which assumes horizontal motions to be independent of distance along the rotation axis, yet accounts for variations in the container height (i.e. the slope of the core–mantle boundary). By projecting the momentum equation onto flows of a QG form, a general equation governing their evolution is derived, which is then adapted for the treatment of two initial value problems—in both Cartesian and spherical geometries—which demonstrate the preference for westward energy propagation by the waves in question. The merits of this mechanism as an explanation for westward drift are discussed.

## 1. Introduction

Since its discovery over three centuries ago by Halley [1], the westward drift of the Earth's magnetic field has remained an intriguing problem in geophysics. Why should it be that many features of the observable geomagnetic field have systematically tracked west throughout 400 years of measurements? The first detailed analysis of this phenomenon was performed by Bullard *et al.* [2], to be followed by many others [3] seeking

THE ROYAL SOCIETY PUBLISHING

to elucidate its behaviour through interrogation of both historical data and recent satellite measurements.

The allure of westward drift can perhaps be put down to its ubiquity. Regardless of whether one looks at maps of declination at the Earth's surface or radial field at the core–mantle boundary, westward drift arises as a robust feature of geomagnetic secular variation. The apparent indifference to both spatial scale [4] and epoch [5] suggests that the westward drift is an artefact of fundamental core dynamics, and therefore its explanation may open a window onto the Earth's deep interior.

While the westward drift spans many temporal and spatial scales, it also appears to be geographically localized, with secular variation being limited to low-latitude (equatorial) regions [5–7], and dominated by the motion of intense flux spots with a tendency to pair north and south of the Equator [8]. For unknown reasons, the Pacific hemisphere appears to have been relatively quiet in the modern era [9], with a weaker field magnitude and lack of any convincing secular variation patterns. The dominant contribution to westward drift—centred over the Equator in the Atlantic hemisphere—was found by Finlay & Jackson [5] to be at a rate of $0.27^\circ\,\mathrm{yr}^{-1}$, or $17\,\mathrm{km\,yr}^{-1}$ at the core–mantle boundary. It is worth noting, however, that these observations face an unfortunate constraint; owing to the interference of crustal magnetism, their resolution is limited to spherical harmonic degrees below 13—meaning there is a dearth of information at all but the largest scales of magnetic field [10]. This is a cause for concern, especially since spectra of the observable secular variation show its power increasing with harmonic degree [4], suggesting its origin is to be found at the invisible small scales. Therefore, theoretical models of the small-scale dynamics may prove useful tools for explaining the westward drift.

The liquid outer core, approximately occupying the spherical shell 1231–3485 km from the Earth's centre, is the cradle of our planet's magnetic field. Its periphery—the core–mantle boundary—may be considered an impermeable, electrically insulating solid on the time scales of interest. Its internal boundary with the solid, conducting inner core will be neglected in this study, as it is thought the geodynamo operates chiefly outside of the tangent cylinder (an imaginary surface aligned with the rotation axis and circumscribing the inner core). The molten iron which makes up the outer core has a kinematic viscosity which is probably not dissimilar to that of water [11], and therefore may be taken as inviscid over the large length scales considered. The force balance is instead thought to be dominated by the effect of the rapid background rotation of the Earth at an angular velocity $\Omega$ of approximately $2\pi$ radians per day. It is well known that rapidly rotating fluids have a tendency to evolve in a manner which is effectively two dimensional, being independent of distance along the rotation axis [12,13], and therefore simplified models which presuppose this disposition are often employed in their study.

Motion in the outer core is thought to be stirred by vigorous convection, with thermally or compositionally buoyant material pushing radially outwards from the hot inner core. The convection is strongly forced, meaning the distribution of density anomaly within the core is likely to be chaotic and span a vast range of scales. This raises questions for both the geodynamo as a whole and the westward drift; how does the organized dipolar field structure emerge from this stochastic forcing, and how can it also produce the systematic drift observed at large scales?

At present, there exist two main schools of thought on the answer to this final question. Arguably the most popular model, due to Pais & Jault [14], invokes a large-scale eccentric gyre—or westward-directed jet—which advects the mean magnetic field. An alternative hypothesis [15–18] rests upon certain magnetohydrodynamic modes with an invariably westward phase velocity. Without remark upon the merits of either of the above models, a third possibility is here put forward, underpinned by the hydrodynamic Rossby waves produced when a rapidly rotating fluid is forced to deviate from two-dimensionality by the presence of the container walls (in this case, the core–mantle boundary). We introduce the quasi-geostrophic (QG) theory of these waves in §2, deriving their governing equation for a general container geometry, and dispersive properties in a canonical example. The waves are linked to westward drift in §3, supported by a simplistic initial value problem. A similar problem is approached in §4, only in a spherical

geometry much more reminiscent of the Earth. The discussion of §5 appraises the value of Rossby waves as a possible source of the observed westward drift.

## 2. Theory of quasi-geostrophic Rossby waves

Consider the Earth's outer core to be an inviscid, incompressible fluid in a state of rapid bulk rotation at an angular velocity $\boldsymbol{\Omega} = \Omega \boldsymbol{e}_z$, where $\boldsymbol{e}_z$ is the unit vector in the axial direction of either a Cartesian $(x, y, z)$ or cylindrical polar $(s, \phi, z)$ co-ordinate system. In either case, a subscript $\perp$ denotes the component of a vector perpendicular to $\boldsymbol{e}_z$. In a reference frame rotating at $\boldsymbol{\Omega}$, the Eulerian fluid velocity is $\boldsymbol{u}(\boldsymbol{x}, t)$. The core–mantle boundary is represented by symmetric, impermeable surfaces at $z = \pm h(\boldsymbol{x}_\perp)$; for a spherical geometry of unit radius, one would have $h = \sqrt{1 - s^2}$.

### (a) Kinematics and the quasi-geostrophic approximation

In a bid to simplify the analysis, the so-called *QG approximation* [19–21] is made. This is in deference to the fact that the rapid background rotation forces the fluid to seek steady states which are independent of the axial co-ordinate $z$ (geostrophic). The presence of the boundaries at $\pm h$ introduces small departures from geostrophy which cause these states to evolve on a time scale much longer than the rotation period; such motions might be called QG, though the definition of the phrase is somewhat imprecise. Here, the term QG is used in a strict sense: as a label for the assumption that the velocity components perpendicular to the rotation axis ($\boldsymbol{u}_\perp$) are independent of the axial co-ordinate, an approach which has seen much success in modelling of outer core convection [22–24]. This is despite the fact that the assumption is only strictly valid when the boundary slope is small, a condition clearly violated in the equatorial regions of the Earth's spherical core [21,25]. Moreover, the approximation remains reasonable even in the presence of a background magnetic field [26].

The velocity field $\boldsymbol{u}$ in this formulation is subject to three kinematic conditions:

(i) incompressibility, $\nabla \cdot \boldsymbol{u} = 0$;
(ii) non-penetration at the upper and lower boundaries, $(\nabla h \mp \boldsymbol{e}_z) \cdot \boldsymbol{u}|_{\pm h} = 0$;
(iii) the QG approximation, $\boldsymbol{u}_\perp = \boldsymbol{u}_\perp(\boldsymbol{x}_\perp, t)$.

It can be shown that a representation of the form

$$\boldsymbol{u} = \nabla \chi \times \nabla \left( \frac{z}{h} \right) \tag{2.1}$$

fulfils these requirements, with the streamfunction $\chi(\boldsymbol{x}_\perp, t)$ neatly encapsulating the evolution of the vector field $\boldsymbol{u}(\boldsymbol{x}, t)$ through a scalar function of just two spatial co-ordinates. Note that this form is a generalization of that introduced by Schaeffer & Cardin [20], which itself improves upon the classical perturbation expansion approach (as discussed in [23]). Restricting solutions to the form (2.1) offers a drastic simplification of the analysis, while providing a useful tool with which to probe the physics of axially elongated structures in the core of the Earth.

### (b) Dynamics and governing equation

A governing equation for the streamfunction $\chi$ in this QG approach is now derived. In a reference frame rotating at the bulk angular velocity $\boldsymbol{\Omega}$, conservation of momentum for an inviscid, incompressible fluid may be written

$$\frac{\partial \boldsymbol{u}}{\partial t} + \boldsymbol{u} \cdot \nabla \boldsymbol{u} + 2\boldsymbol{\Omega} \times \boldsymbol{u} = -\nabla \Pi \tag{2.2}$$

for some modified pressure $\Pi$. In the limit of small Rossby number ($\mathcal{U} \ll \Omega \mathcal{L}$ for some characteristic velocity $\mathcal{U}$ and length scale $\mathcal{L}$), the second term (advection) may be neglected in

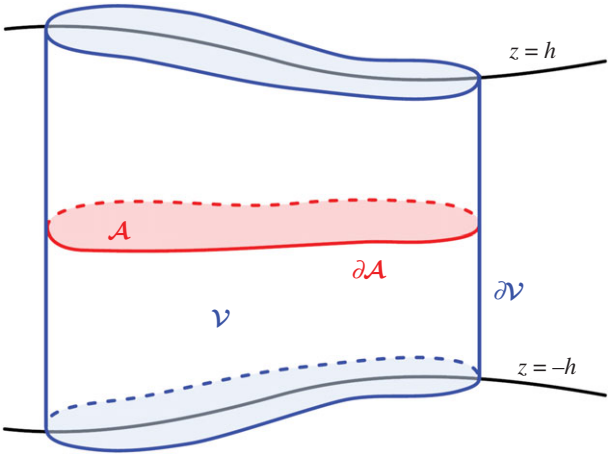


**Figure 1.** Schematic of the control volume considered when deriving the governing equation for a QG flow. (Online version in colour.)

comparison with the third (Coriolis). The curl of (2.2) then yields the equation

$$\frac{\partial \boldsymbol{\omega}}{\partial t} = 2\boldsymbol{\Omega} \cdot \nabla \boldsymbol{u}, \tag{2.3}$$

for the evolution of the vorticity $\boldsymbol{\omega} = \nabla \times \boldsymbol{u}$. Evidently, steady solutions must be independent of distance along the rotation axis (i.e. geostrophic)—this is the Taylor–Proudman theorem [12,13]. However, in order to satisfy non-penetration at $z = \pm h$, QG solutions must possess a weak $z$-dependence, and therefore can exhibit unsteadiness. To derive an equation for the evolution of a QG flow, one could simply substitute the representation (2.1) into the axial component of the vorticity equation (2.3), a procedure commonly employed in the literature (e.g. [21,22]). However, as pointed out in Labbé *et al.* [27], a more efficacious approach is to instead project the momentum equation (2.2) onto flows of the QG form (2.1), thereby obtaining a reduced model which better approximates the dynamics. This has been verified analytically in a full sphere by Maffei *et al.* [25], who found remarkably good agreement with the fully three-dimensional solutions of Zhang *et al.* [28].

We therefore proceed by following the derivation of Labbé *et al.* [27], generalizing their results in a sphere to a more arbitrary geometry. Consider a control volume $\mathcal{V}$ of fluid of constant horizontal cross section $\mathcal{A}$, bounded at the top and bottom by the caps $z = \pm h(\boldsymbol{x}_\perp)$. The boundaries of $\mathcal{V}$ and $\mathcal{A}$ are denoted $\partial\mathcal{V}$ and $\partial\mathcal{A}$, respectively (figure 1). After excluding advection, the momentum equation (2.2) is projected onto a QG trial function $\boldsymbol{u}' = \nabla\chi' \times \nabla(z/h)$, which by construction satisfies $\chi'|_{\partial\mathcal{A}} = 0$, then integrated over $\mathcal{V}$:

$$\iiint_{\mathcal{V}} \boldsymbol{u}' \cdot \dot{\boldsymbol{u}}\, \mathrm{d}V + 2\Omega \iiint_{\mathcal{V}} \boldsymbol{u}' \cdot (\boldsymbol{e}_z \times \boldsymbol{u})\, \mathrm{d}V = -\iiint_{\mathcal{V}} \boldsymbol{u}' \cdot \nabla \Pi\, \mathrm{d}V, \tag{2.4}$$

with a dot over a quantity denoting a time derivative. Using the divergence theorem, the right-hand side is equal to

$$\iiint_{\mathcal{V}} \Pi \nabla \cdot \boldsymbol{u}'\, \mathrm{d}V - \oiint_{\partial\mathcal{V}} \Pi \boldsymbol{u}' \cdot \mathrm{d}\boldsymbol{S} = 0, \tag{2.5}$$

as the choice of $\chi'$ guarantees streamlines of $\boldsymbol{u}'$ cannot pass through $\partial\mathcal{V}$. The contribution from the Coriolis term simplifies to

$$2\Omega \iiint_{\mathcal{V}} \boldsymbol{u}' \cdot (\boldsymbol{e}_z \times \boldsymbol{u})\, \mathrm{d}V = 2\Omega \iiint_{\mathcal{V}} \left(\frac{\boldsymbol{e}_z \times \nabla\chi}{h^2}\right) \cdot \nabla\chi'\, \mathrm{d}V. \tag{2.6}$$

The integration from $z=-h$ to $z=h$ can be completed, thereby projecting the equations onto the horizontal plane $\mathcal{A}$:

$$2\Omega \iiint_{\mathcal{V}} \boldsymbol{u}' \cdot (\boldsymbol{e}_z \times \boldsymbol{u})\,\mathrm{d}V = 4\Omega \iint_{\mathcal{A}} \left(\frac{\boldsymbol{e}_z \times \nabla\chi}{h}\right) \cdot \nabla\chi'\,\mathrm{d}A \tag{2.7}$$

$$= 4\Omega \oint_{\partial\mathcal{A}} \chi' \left(\frac{\boldsymbol{e}_z \times \nabla\chi}{h}\right) \cdot \boldsymbol{n}\,\mathrm{d}s - 4\Omega \iint_{\mathcal{A}} \chi' \nabla \cdot \left(\frac{\boldsymbol{e}_z \times \nabla\chi}{h}\right) \mathrm{d}A \tag{2.8}$$

$$= 4\boldsymbol{\Omega} \cdot \iint_{\mathcal{A}} \chi' \left(\nabla\frac{1}{h} \times \nabla\chi\right) \mathrm{d}A. \tag{2.9}$$

This requires use of the two-dimensional version of the divergence theorem,

$$\iint_{\mathcal{A}} \nabla \cdot \boldsymbol{v}\,\mathrm{d}A = \oint_{\partial\mathcal{A}} \boldsymbol{v} \cdot \boldsymbol{n}\,\mathrm{d}s \tag{2.10}$$

(where $\boldsymbol{n}$ is the in-plane unit outward normal to $\partial\mathcal{A}$), then the fact that $\chi'|_{\partial\mathcal{A}} = 0$. A very similar procedure may be applied to the inertial term,

$$\iiint_{\mathcal{V}} \boldsymbol{u}' \cdot \dot{\boldsymbol{u}}\,\mathrm{d}V = \iiint_{\mathcal{V}} \left(\frac{\nabla\dot{\chi}}{h^2} + z^2\nabla\frac{1}{h} \times \left(\nabla\dot{\chi} \times \nabla\frac{1}{h}\right)\right) \cdot \nabla\chi'\,\mathrm{d}V \tag{2.11}$$

$$= 2\iint_{\mathcal{A}} \left(\frac{\nabla\dot{\chi}}{h} + \frac{h^3}{3}\nabla\frac{1}{h} \times \left(\nabla\dot{\chi} \times \nabla\frac{1}{h}\right)\right) \cdot \nabla\chi'\,\mathrm{d}A \tag{2.12}$$

$$= -2\iint_{\mathcal{A}} \chi' \nabla \cdot \left(\frac{\nabla\dot{\chi} + (1/3)\nabla h \times (\nabla\dot{\chi} \times \nabla h)}{h}\right) \mathrm{d}A, \tag{2.13}$$

so equation (2.4) can be rewritten

$$\iint_{\mathcal{A}} \chi' \left[\nabla \cdot \left(\frac{\nabla\dot{\chi} + (1/3)\nabla h \times (\nabla\dot{\chi} \times \nabla h)}{h}\right) + 2\boldsymbol{\Omega} \cdot \left(\nabla\chi \times \nabla\frac{1}{h}\right)\right] \mathrm{d}A = 0. \tag{2.14}$$

As this must be satisfied for all possible choices of the trial function $\chi'$, the streamfunction $\chi$ must obey the governing equation

$$\nabla \cdot \left(\frac{\nabla\dot{\chi} + (1/3)\nabla h \times (\nabla\dot{\chi} \times \nabla h)}{h}\right) + 2\boldsymbol{\Omega} \cdot \left(\nabla\chi \times \nabla\frac{1}{h}\right) = 0. \tag{2.15}$$

Note that the second term inside the divergence is the sole difference between this equation and the axial vorticity formulation (i.e. plugging (2.1) into the $z$-component of (2.3)); for moderate values of $\nabla h$, however, this difference becomes significant.

## (c) Quasi-geostrophic Rossby waves

The governing equation (2.15) can support oscillatory solutions known as QG Rossby waves, in analogy to their atmospheric counterparts [15,29], discussed in detail by Vallis [30], for example. The theory of QG Rossby waves in the Earth's interior mirrors this classical analysis—to extract their archetypal form, select Cartesian co-ordinates $(x, y, z)$ and a linear height profile $h(y) = H + h'y$ for positive constants $H$ and $h'$, the domain height and slope, respectively. This aims to capture the slope of the core–mantle boundary at zero order, with the $x$-axis oriented east and the $y$-axis radially inwards. Furthermore, the slope is for the moment assumed small (in comparison with the aspect ratio of the QG structures), so (2.15) may be written in the linearized form

$$\frac{\partial}{\partial t}\nabla^2\chi \approx \frac{2\Omega h'}{H}\frac{\partial\chi}{\partial x}. \tag{2.16}$$

Note that an equivalent equation could also stem from the axial vorticity formulation, or indeed a perturbation expansion approach [31]. Seek travelling wave solutions of the form $\chi(x, y, t) \propto \exp\{\mathrm{i}(\boldsymbol{k}_\perp \cdot \boldsymbol{x}_\perp - \varpi(\boldsymbol{k}_\perp)t)\}$ with frequency $\varpi$ and wavevector $\boldsymbol{k}_\perp = [k_x, k_y, 0]^{\mathrm{T}} = k_\perp[\cos\alpha, \sin\alpha, 0]^{\mathrm{T}}$,

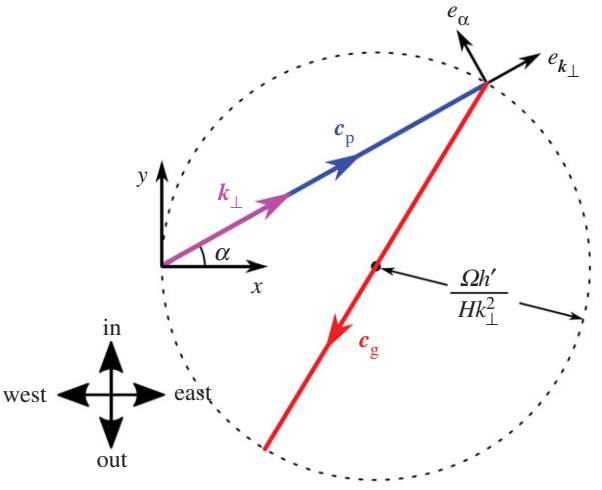


**Figure 2.** Velocity diagram for QG Rossby waves when $h = H + h'y$ for small $h'$. Phase velocity $\boldsymbol{c}_p$ is related to group velocity $\boldsymbol{c}_g$ for a given choice of $\boldsymbol{k}_\perp$. The rotation axis is out of the page, and the labelled directions orient the figure within the Earth's outer core. (Online version in colour.)

where $\alpha$ is the angle between the wavevector and the $x$-axis and $k_\perp = |\boldsymbol{k}_\perp|$. This yields the dispersion relationship for QG Rossby waves

$$\varpi = \frac{2\Omega h'}{Hk_\perp}\cos\alpha. \tag{2.17}$$

Writing $\boldsymbol{e}_{k_\perp}$ for the unit vector in the direction of $\boldsymbol{k}_\perp$ and $\boldsymbol{e}_\alpha$ for the unit vector in the direction of increasing $\alpha$ (figure 2), the phase velocity corresponding to (2.17) can be expressed as

$$\boldsymbol{c}_p = \frac{\varpi}{k_\perp}\boldsymbol{e}_{k_\perp} = \frac{2\Omega h'}{Hk_\perp^2}\cos\alpha\ \boldsymbol{e}_{k_\perp}. \tag{2.18}$$

Note that the component of phase velocity in the $x$-direction is always positive, meaning wave crests invariably progress eastwards. However, the same is not true for the wave energy, which instead propagates at the group velocity, given by the gradient in $\boldsymbol{k}_\perp$-space of the frequency,

$$\boldsymbol{c}_g = \frac{\partial\varpi}{\partial k_\perp}\boldsymbol{e}_{k_\perp} + \frac{1}{k_\perp}\frac{\partial\varpi}{\partial\alpha}\boldsymbol{e}_\alpha = -\frac{2\Omega h'}{Hk_\perp^2}(\cos\alpha\ \boldsymbol{e}_{k_\perp} + \sin\alpha\ \boldsymbol{e}_\alpha). \tag{2.19}$$

The relationship between the phase and group velocities is best understood diagrammatically; figure 2 is a velocity diagram relating the two, similar to the plots of Duba & McKenzie [32]. The magnitude of $\boldsymbol{c}_g$ is independent of $\alpha$, so on the velocity diagram the vector $\boldsymbol{c}_g$ is the diameter of a circle of radius $\Omega h'/Hk_\perp^2$. Furthermore, $(\boldsymbol{c}_p + \boldsymbol{c}_g)\cdot\boldsymbol{c}_p = 0$, so $\boldsymbol{c}_p$ is a chord of the same circle terminating at the base of $\boldsymbol{c}_g$. As $\boldsymbol{c}_p$ is always in the positive $x$-direction, the circle must lie to the right of the origin as shown.

Using figure 2, it is possible to probe the effect of varying the wavevector orientation $\alpha$ for a given $k_\perp$ (i.e. a specified horizontal length scale). Consider only positive frequencies ($-\pi/2 < \alpha \leq \pi/2$), for which figure 2 makes sense. The phase velocity vector $\boldsymbol{c}_p$ is constrained to move along the dashed circle, whereas the group velocity vector $\boldsymbol{c}_g$ starts where $\boldsymbol{c}_p$ finishes and is necessarily a diameter of the same circle. Although the phase velocity always has a positive $x$-component, the group velocity shows no such preference. In fact, the $x$-component of $\boldsymbol{c}_g$ is negative (westward) for $|\alpha| < \pi/4$ and positive (eastward) for $|\alpha| > \pi/4$. When $\alpha = 0$, $\boldsymbol{c}_p$ and $\boldsymbol{c}_g$ are exactly opposite, so an observer following a wave group moving westward would see wave crests heading in the opposite direction at twice the speed of the group. When $\alpha = \pi/2$ the group velocity remains finite

(and due east) despite the fact the waves have no phase velocity. Waves with $\alpha = \pi/4$ propagate directly outwards and waves with $\alpha = -\pi/4$ inwards.

The dependence of wave velocity on $k_\perp$ is comparatively trivial; waves with longer wavelengths (smaller $k_\perp$) travel faster. As $|c_g| \sim k_\perp^{-2}$, the waves are highly dispersive.

## 3. Quasi-geostrophic Rossby waves and the westward drift

A possible explanation for the westward drift of the Earth's magnetic field at the core–mantle boundary based upon this classical theory of hydrodynamic QG Rossby waves is now offered. Suppose, not unreasonably, that the fluid outer core is stirred by gravitating buoyant anomalies, which constitute localized disturbances to the system in the form of convective upwellings or plumes. Consider one such disturbance introduced at a location outside of the tangent cylinder (i.e. not directly north or south of the solid inner core). The disturbance will in general be three dimensional, but the velocity field it instigates will rapidly become elongated along the rotation axis through the action of inertial waves [33], and therefore QG after a short transient period. It is thus useful to consider a thought experiment posed as an initial value problem in which a localized QG velocity field is specified as an initial condition, and the flow allowed to evolve as an assemblage of QG Rossby waves, operating on a time scale much longer than the rotation period.

A generic initial condition will excite a broad spectrum of waves—that is to say, many different choices of wavevector $\boldsymbol{k}_\perp$—which will all spread from the source according to their individual dispersive properties. A disturbance of characteristic size $\ell$ will have a spectrum peaked around a wavevector magnitude $k_\perp$ of order $\ell^{-1}$, but will in general excite wavevectors of all possible orientations $\alpha$. Therefore, consider the dependence of the group velocity on wavevector orientation by referring back to figure 2. For wavevectors with $\alpha \approx \pm\pi/2$, corresponding to structures elongated in the east–west direction, the group velocity is east; for wavevectors with $\alpha \approx 0$, i.e. structures elongated in the radial direction, the group velocity is west. QG Rossby waves, therefore, disperse in a manner which segregates different spatial structures from an arbitrary initial disturbance, with east–west extended features heading east and radially-extended features west.

However, it is unreasonable to assume that the excitation of these waves in the core of the Earth is arbitrary. For motions continually stirred by vigorous convection, one might expect the proliferation of sinuous radial plumes, emanating from the inner core and being much longer than they are wide. Such structures commonly arise in numerical and experimental studies of core dynamics (e.g. [34,35]). Owing to the constraint imposed by the rapid background rotation, such plumes would also be elongated in the axial direction, forming a series of radial sheets which are likely to be well represented by the QG approximation [36]. In the context of our thought experiment, a radial sheet (extended in the $y$-direction) will possess much more energy in wavevectors pointing east–west ($\alpha \approx 0$) than radially ($\alpha \approx \pm\pi/2$). When the solution to such an initial value problem is evolved, the abundance of wavevectors with $\alpha \approx 0$ will dominate the picture. As the group velocity for these solutions is in the negative $x$-direction, a radially-extended disturbance will preferentially transmit energy to the west, making this class of QG Rossby waves an intriguing candidate for the mechanism underlying westward drift.

### (a) Demonstration through a model problem

To support the arguments made so far, consider a simplistic model problem which demonstrates the ability of QG Rossby waves to segregate different spatial structures. The canonical equation (2.16) is solved in a domain which is infinite in $x$ and $y$, starting from some initial condition $\chi(\boldsymbol{x}_\perp, t = 0) = \chi_{\text{init}}(\boldsymbol{x}_\perp)$, by taking a two-dimensional spatial Fourier transform. Emphasis is placed upon the significance of the choice of initial condition, which is constrained to be of the form

$$\chi_{\text{init}} = \exp\left\{-\frac{1}{2}\left(\frac{x^2}{\ell_x^2} + \frac{y^2}{\ell_y^2}\right)\right\}. \tag{3.1}$$

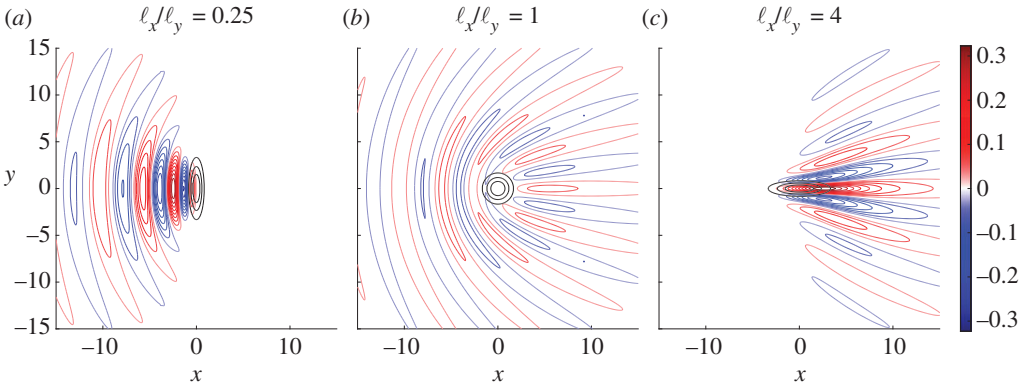


**Figure 3.** Solutions to the canonical QG Rossby wave equation (2.16) for a simple initial value problem starting from (3.1). The height of the container is $h = H + h'y$. Contours of streamfunction $\chi$ are plotted at $2\Omega h' t/H = 15$ for three different choices of aspect ratio, and black contours are at quartiles of the initial condition. Lengths are in units of $\sqrt{\ell_x \ell_y}$. (Online version in colour.)

As contours of $\chi$ are equivalent to streamlines in the equatorial plane, this corresponds to a columnar vortex of extent $\ell_x$ in the $x$-direction and $\ell_y$ in the $y$-direction. Using $\sqrt{\ell_x \ell_y}$ as the unit of length, the solution to the initial value problem may be written as the two-dimensional dispersion integral

$$\chi(\boldsymbol{x}_\perp, t) = \frac{2}{\pi} \int_0^{\pi/2} \int_0^{\infty} k_\perp \exp\left\{-\frac{1}{2} k_\perp^2 (\ell_x^2 \cos^2\alpha + \ell_y^2 \sin^2\alpha)\right\} \times \cos\left(\left[k_\perp x - \frac{2\Omega h' t}{H k_\perp}\right] \cos\alpha\right) \cos(k_\perp y \sin\alpha)\, \mathrm{d}k_\perp\, \mathrm{d}\alpha, \tag{3.2}$$

wherein $k_\perp$ and $\alpha$ have the same interpretations as in the dispersion relation (2.17). This expression is evaluated numerically for three different choices of the initial condition's aspect ratio $\ell_x/\ell_y$ (figure 3). Figure 3*b* shows the case of an axisymmetric initial condition, which excites waves of all orientations $\alpha$ equally and therefore shows no preferential direction for energy transport, although the partition of different spatial structures is visible. Figure 3*a* shows the case of a radially-extended initial condition, four times longer in the direction of the slope than it is wide; the bias towards westward-propagating waves is self-evident. For completeness, figure 3*c* features an initial condition which is elongated in the east–west direction, which exhibits a strong preference for eastward propagation. It is worth remarking that the aspect ratio need not be extreme for this effect to be apparent; it is very clear-cut here even for a moderate value of 4 : 1.

## 4. A model problem: westward-propagating waves in a sphere

It has been established so far that, in the case of a gentle slope, the linearized equation (2.16) supports wave motions which partition different spatial structures—crucially, with flows elongated in the direction of the slope going west. However, it is not obvious that the same will necessarily hold true for a more complicated geometry with an appreciable slope, such as that presented by the core–mantle boundary. Therefore, consider an initial value problem similar to that of the previous section, but in an enclosed spherical geometry reminiscent of the Earth's core. A full sphere—deficient of the solid inner core—is used in order to simplify the analysis. First, mode shapes and frequencies are derived in this geometry, following Maffei *et al.* [25], before the calculated modes are used to solve an illustrative initial value problem.

Despite the spherical geometry, cylindrical polar coordinates $(s, \phi, z)$—with $s$ being the radial location, $\phi$ the azimuthal angle and $z$ the distance along the rotation axis—are adopted in order to

usefully apply the QG approximation. Taking lengths in units of outer core radii, the governing equation is then (2.15) with the axisymmetric height profile $h(s)=\sqrt{1-s^2}$,

$$\left[\frac{\partial}{\partial s}\left(\frac{s}{h}\frac{\partial}{\partial s}\right)+\frac{1}{hs}\left(1+\frac{s^2}{3h^2}\right)\frac{\partial^2}{\partial\phi^2}\right]\frac{\partial\chi}{\partial t}-\frac{2\Omega s}{h^3}\frac{\partial\chi}{\partial\phi}=0. \tag{4.1}$$

First, note that any solution satisfying $\partial\chi/\partial t=\partial\chi/\partial\phi=0$ will be a particular integral of this equation. This corresponds to the steady, strictly geostrophic motion of coaxial cylinders ($\boldsymbol{u}=u_\phi(s)\boldsymbol{e}_\phi$); hence, the axisymmetric component of any initial condition will not evolve, and one need only solve (4.1) for the non-axisymmetric portion of the flow. This can be done by seeking normal mode solutions of the form

$$\chi(s,\phi,t)=\mathbb{R}\{\bar{\chi}(s)\exp(\mathrm{i}[m\phi-\varpi t])\}, \tag{4.2}$$

for some azimuthal wavenumber $m$ and modal frequency $\varpi$, with $\mathbb{R}\{\cdot\}$ denoting the real part of a quantity. This turns (4.1) into an ordinary differential equation for the radial mode shape,

$$\frac{\mathrm{d}}{\mathrm{d}s}\left(\frac{s}{h}\frac{\mathrm{d}\bar{\chi}}{\mathrm{d}s}\right)+\left[\frac{2\Omega ms}{\varpi h^3}-\frac{m^2}{hs}\left(1+\frac{s^2}{3h^2}\right)\right]\bar{\chi}=0, \tag{4.3}$$

which must be solved subject to boundary conditions at the origin ($s=0$) and the equatorial boundary ($s=1$). Regularity at the origin requires $\bar{\chi}\sim s^m$ as $s\to 0$, whereas non-penetration at the outer boundary requires

$$u_s|_{s=1}=\lim_{s\to 1}\left(\frac{1}{hs}\frac{\partial\chi}{\partial\phi}\right)=0. \tag{4.4}$$

As $\chi$ is a streamfunction, its constant value at the outer boundary can be chosen, so is set at zero; more specifically, we must have $\bar{\chi}(s\to 1)\sim h^3$ in order for $u_s=(1/hs)(\partial\chi/\partial\phi)$ to be zero and $u_\phi=-(1/h)(\partial\phi/\partial s)$ to be finite at the outer boundary. The solution to the eigenvalue problem posed by (4.3) and these boundary conditions is given in Maffei *et al.* [25]; the mode shapes are of the form

$$\bar{\chi}_n^m(s)=s^m h^3 P_{n-1}^{(3/2,m)}(2s^2-1), \tag{4.5}$$

and the corresponding frequencies are

$$\varpi_n^m=\frac{m}{n(2n+2m+1)+m/2+m^2/6}. \tag{4.6}$$

Here, $n\geq 1$ is the radial mode number, equal to the number of turning points of $\bar{\chi}_n^m$ within the domain. The mode shapes are expressed in terms of Jacobi polynomials $P_\nu^{(\alpha,\beta)}(x)$ [37]. Note that, for all $m\geq 1$, the frequency $\varpi_n^m$ is positive, meaning all modes revolve in a prograde (eastward) sense; this is analogous to the observation that the phase velocity in the Cartesian problem (2.18) is always in the positive $x$-direction. Just as in that problem, this does not preclude the possibility that the energy from a localized disturbance can nevertheless propagate west, as demonstrated below.

The general solution to (4.1) (setting aside the axisymmetric particular integral for a moment) can be written as an infinite sum of the above modes,

$$\chi(s,\phi,t)=\mathbb{R}\left\{\sum_{m=1}^{\infty}\sum_{n=1}^{\infty}C_n^m\bar{\chi}_n^m(s)\,\mathrm{e}^{\mathrm{i}(m\phi-\varpi_n^m t)}\right\} \tag{4.7}$$

for some complex coefficients $C_n^m$ to be determined by the initial condition $\chi_{\mathrm{init}}(s,\phi)$. In fact, it can be seen from the self-adjoint equation (4.3) that the radial mode shapes (4.5) are orthogonal with

respect to the function $s/h^3$, i.e.

$$\int_0^1 \frac{s}{h^3}\,\bar{\chi}_n^m(s)\bar{\chi}_{n'}^m(s)\,\mathrm{d}s = 0 \quad \text{for } n \neq n', \tag{4.8}$$

which enables the derivation of an expression for each modal coefficient as an integral over the equatorial plane,

$$C_n^m = \frac{\int_0^1 (s/h^3)\bar{\chi}_n^m(s)\oint \chi_{\mathrm{init}}(s,\phi)\,\mathrm{e}^{-\mathrm{i}m\phi}\,\mathrm{d}\phi\,\mathrm{d}s}{\pi\int_0^1 (s/h^3)[\bar{\chi}_n^m(s)]^2\,\mathrm{d}s}. \tag{4.9}$$

All that remains is the axisymmetric portion of the flow, given simply by

$$\chi_{\mathrm{ax}}(s) = \frac{1}{2\pi}\oint \chi_{\mathrm{init}}(s,\phi)\,\mathrm{d}\phi. \tag{4.10}$$

This analysis allows the solution of an illustrative initial value problem, similar to that of §3, by using (4.9) to express the initial condition as a linear sum of modes and solving for the streamfunction at a later time by evaluating the sums in (4.7) truncated at finite $m$ and $n$.

## (a) Choice of initial condition

If the simple Cartesian cartoon discussed in §3 is to be believed, the choice of initial condition, and therefore distribution of energy in $\boldsymbol{k}_\perp$-space (or, equivalently, between modes), will have a profound effect on the direction of net energy propagation. In fact, those modes for which the frequency $\varpi_n^m$ in (4.6) is a decreasing function of $m$ will be associated with westward propagation of energy; in the Cartesian case, $c_{g,x}$ is negative for $\partial\varpi/\partial k_x < 0$, and analogously retrograde group velocity is seen in the sphere for $\partial\varpi_n^m/\partial m < 0$, i.e.

$$m > \sqrt{6n(1+2n)}. \tag{4.11}$$

For a westward drift to be observed in this model problem, the harmonic content of the initial condition must be biased towards modes which satisfy this inequality. For definiteness, discussion is restricted to the form of initial condition

$$\chi_{\mathrm{init}}(s,\phi) = h^3 s\,\exp\left\{-\frac{1}{2}\left(\frac{(s-s_0)^2}{\ell_s^2} + \frac{s_0^2\phi^2}{\ell_\phi^2}\right)\right\}. \tag{4.12}$$

This is essentially a columnar Gaussian vortex, as for the model problem of §3, with the pre-multiplying factor $h^3 s$ ensuring the boundary conditions are satisfied from the outset. It is broadly unimportant exactly what form the initial condition takes, however— it is the general distribution of energy between modes which will dictate the solution's character.

There are three controlling lengths in the initial condition (4.12); the radial and azimuthal extents of the vortex $\ell_s$ and $\ell_\phi$, and the radial location of the vortex centre $s_0$. In search of a westward bias to energy propagation, the parameters $\ell_s = 0.1$, $\ell_\phi = 0.01$ and $s_0 = 0.7$ are selected, giving a slender radially-extended structure near the middle of the outer core region $0.35 < s < 1$ (though there is no inner core boundary in this calculation). The solution is expressed as a finite sum of modes (i.e. a truncated version of (4.7)) by evaluating the integrals (4.9) for the coefficients $C_n^m$ numerically. Owing to the narrowness of the initial condition, more modes of high azimuthal wavenumber are required; the ranges $m \leq 200$ and $n \leq 50$ are used.

## (b) Westward bias to energy propagation in a sphere

Figure 4 shows the solution to the initial value problem evaluated at $\Omega t = 2\times 10^4$ ($t = 8.7$ yr). Streamlines in the equatorial plane are produced by plotting contours of $\chi$, with the black contours corresponding to the initial value (4.12). Although this solution is many times more complicated than the Cartesian problem of figure 3, there remains a striking preference for wave propagation to the west of the initial disturbance. This is despite the fact that each individual eigenmode has an eastward phase velocity; it is the superposition of modes which creates the

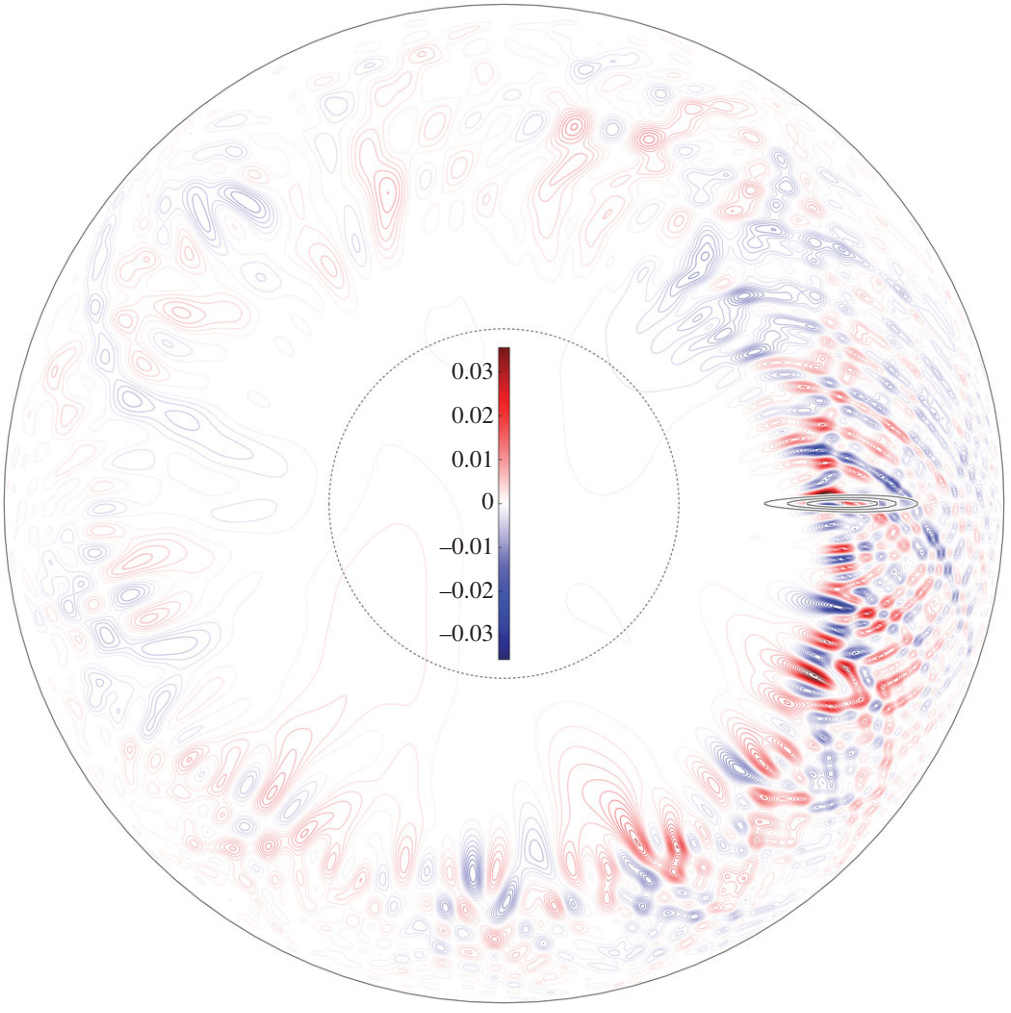


**Figure 4.** Contours of $\chi$ (i.e. streamlines in the equatorial plane, viewed from the north) at $\Omega t = 2 \times 10^4$ for an initial value problem starting from a radially-extended vortex (4.12) with $\ell_s = 0.1$, $\ell_\phi = 0.01$ and $s_0 = 0.7$. Solid black contours are at quartiles of the initial condition, and the dashed black line shows the would-be location of the solid inner core. (Online version in colour.)

visible westward bias. Wave motion appears to be confined to a circular band near the initial radial location $s_0$, with little activity very close to the outer boundary or near the rotation axis. The dashed line is at $s = 0.35$, where the inner core would be if it were included in the model; thankfully, the vast majority of activity occurs outside of this region.

The preference for westward propagation may be understood in exactly the same way as the Cartesian problem of §3, but with the small slope assumption now relaxed. The majority of the energy from the radially-extended initial condition is contained in modes with large azimuthal wavenumbers, which conspire to produce a westward group velocity despite individually having eastward phase velocities. To demonstrate that the former prevails, consider the distribution of energy in the sphere as a function of longitude and time. Namely, the meridionally averaged specific kinetic energy,

$$\left\langle \frac{1}{2}\boldsymbol{u}^2 \right\rangle (\phi, t) = \int_0^1 \left( \int_{-h}^{h} \frac{1}{2}\boldsymbol{u}^2 \, \mathrm{d}z \right) s \, \mathrm{d}s = \int_0^1 \frac{s}{h} \left[ (\nabla\chi)^2 + \frac{1}{3}(\nabla\chi \times \nabla h)^2 \right] \mathrm{d}s, \tag{4.13}$$

is evaluated as a function of $\phi$ at a few choice times (figure 5). The energy, initially localized around $\phi = 0$, is almost all at negative $\phi$ when $\Omega t = 2 \times 10^3$, and is still sharply peaked as

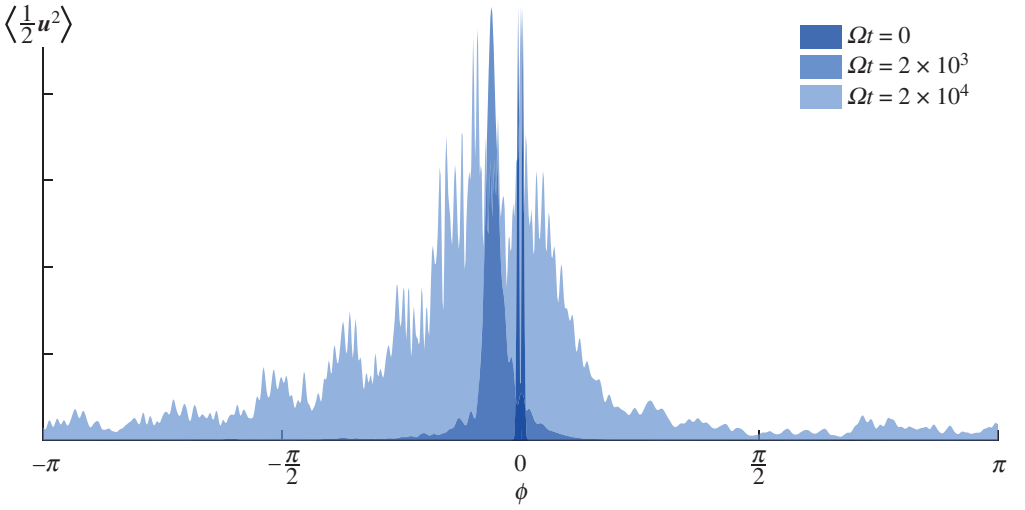


**Figure 5.** Specific kinetic energy, averaged over meridional slices, as a function of longitude $\phi$ for the initial condition and two later times $\Omega t = 2 \times 10^3$ and $\Omega t = 2 \times 10^4$. Plots are normalized to have the same maxima, though in actuality they contain equal areas. (Online version in colour.)

the waves have had little time to disperse. Come $\Omega t = 2 \times 10^4$, which corresponds to figure 4, the energy is much more dispersed but retains its westward bias; of course, reflections and circumnavigations mean a little energy does end up to the east of the initial disturbance.

## 5. Discussion

The model problems above successfully demonstrate the possibility for westward transport of energy by hydrodynamic QG Rossby waves, but are intended as a proof-of-concept rather than an accurate representation of core dynamics. Clearly, the flow in the Earth's outer core is not the solution to an initial value problem, but rather the result of continual convective stirring; the interplay between buoyancy and velocity fields will introduce complexity beyond the scope of this study [24]. However, the present theory demonstrates that westward propagation requires only the prevalence of radial plumes, which are likely to be robustly generated by the buoyant upwellings associated with strongly forced convection.

Indeed, discussions of vigorously forced convection are intrinsically linked to the relevant smallest length scale in the core of the Earth, which is itself pertinent to dynamo action [38]. The thickness of the radial plumes will have a strong bearing on the propagation speed of their associated wave packets, as the magnitude of the group velocity (2.19) is proportional to the square of the wavelength, meaning narrower structures propagate much slower. The most strongly forced simulations to date (e.g. [34]) show structures more slender than those considered in the model problem of figure 4, and it is not unreasonable to suspect that the true length scale is even smaller. In fact, it is possible to infer this length scale under the assumption that QG Rossby waves are responsible for the westward drift. From the expression for group velocity (2.19), the speed of a wavepacket at a certain cylindrical radius $s$ is given by

$$|\boldsymbol{c}_g| \approx \frac{2\Omega}{hk_\perp^2}\left|\frac{\mathrm{d}h}{\mathrm{d}s}\right| = \frac{2\Omega s}{(hk_\perp)^2}. \tag{5.1}$$

For an azimuthally propagating wavepacket, the angular velocity about the rotation axis is $|\boldsymbol{c}_g|/s$; equating this to the observed drift rate of the magnetic field $D$ gives an expression for the dominant wavelength of the packet,

$$\lambda \approx 2\pi h\sqrt{\frac{D}{2\Omega}}. \tag{5.2}$$

Using a drift rate of 0.27° per year [5] and a radial location of the wavepacket $s \sim 2000$ km gives the estimate $\lambda \sim 18$ km, a conceivable value for the prevalent scales in the Earth's core, but one which should be treated with caution. Firstly, it is within touching distance of the Rhines length $\sqrt{\mathcal{U}h/\Omega}$ (approx. 6 km for $\mathcal{U} \sim 1\,\mathrm{mm\,s^{-1}}$), at which the advection term in (2.2) becomes significant and mean flows may arise. Secondly, the aspect ratios of such structures would be improbably large for their coherence to be maintained over secular time scales. It seems more reasonable that in truth $\lambda$ is greater, with additional factors—interactions with the buoyancy and magnetic fields, large values of boundary slope or departures from quasi-geostrophy—acting to slow the wave groups down. Unfortunately, the machinery required to investigate these nonlinear phenomena lies beyond our present scope.

Nevertheless, it seems remiss that so far no consideration has been given to the magnetic field, despite the fact that the observed westward drift of its large-scale features is the motivation for this study. It is therefore necessary to ask what could link hydrodynamic QG Rossby waves to the apparent motion of the spherical radial magnetic field $B_\mathrm{r}$ at the core–mantle boundary. Since the drift is observed to be mainly in the equatorial regions [8], motion of the *cylindrical* radial field $B_s$, which will be approximately equal to $B_\mathrm{r}$ at low latitudes, is discussed instead. To a first approximation, magnetic field lines may be thought of as material curves, pinned into the fluid at all points [29,39], so there are essentially two ways of modifying the radial magnetic field: advection and stretching of an existing $B_s$ by a mean flow, or rotation of the other components ($B_\phi$, $B_z$) by transverse gradients in radial velocity ($\partial_\phi u_s$, $\partial_z u_s$ respectively); both mechanisms are discussed in the context of westward drift by Finlay [40] and Aubert *et al.* [41]. Westward-propagating QG Rossby waves, which necessarily consist of radially-extended sheet-like structures, have small azimuthal velocities so are unlikely to advect $B_s$ strongly enough to account for the westward drift. The radial velocity is much greater, but has small derivatives in $s$ and $z$ so stretching of an existing $B_s$ or shearing of $B_z$ are both unlikely mechanisms. The best candidate for generation of $B_s$ is therefore shearing of $B_\phi$ by azimuthal gradients in $u_s$, which are large for the slender radial jets. Furthermore, the azimuthal magnetic field is likely to be relatively strong within the core [42], and largest at mid- to low latitudes—which could explain the equatorial bias to the observed drift, since a low-latitude $B_\phi$ swept out by a QG radial jet would produce a radial field anomaly at the core–mantle boundary in the vicinity of the Equator.

At first glance, this argument appears to suffer from the deficiency that the manipulation of $B_s$ occurs on the small scale of the wavelength $\lambda$, whereas the observed drift occurs in magnetic field features hundreds of kilometres across. However, the observations themselves are hampered by a lack of spatial resolution, so small-scale features simply are not visible, even though they may in fact contain a significant portion of the energy [4]. The observations instead feature large, westward-moving patches [8] which one might compare to wave groups, with the small-scale details (wave crests and troughs) within each patch unavailable. It is therefore to be expected that, if the present theory were to explain the observations, large magnetic field features would appear to be advected at the group (rather than phase) velocity of QG Rossby wave packets.

The feedback of the magnetic field on the dynamics through the action of the Lorentz force has been ignored in this study. Indeed, for highly simplified field configurations it has been shown that its inclusion introduces additional oscillations known as *slow magnetic Rossby waves* which themselves have been suggested as a possible source of magnetic field drift since their phase velocity is always westward [15–18]. However, these slow solutions coexist with others known as *fast magnetic Rossby waves*, which are little more than a weakly modified version of the hydrodynamic solutions discussed at length above. The perturbation to the magnetic field does not strongly influence the dynamics of these waves, and so they remain an equally viable source of westward drift, with the magnetic field approximating a passive tracer at leading order.

Moreover, the fact that the dynamics of QG Rossby waves are independent of the magnetic field configuration and magnitude is a strength of the present theory. Slow magnetic Rossby modes have to date only been demonstrated for simple choices of background field [21,27], and it is therefore unclear whether such solutions are meaningful in a geophysical context.

Conversely, the fast (i.e. hydrodynamic) solutions are likely to persist regardless of the magnetic field structure, meaning they are an almost unavoidable feature of QG flows in the Earth's outer core. This robustness tallies with the observation of westward drift as a systematic component of the geomagnetic secular variation, and the fact that the waves operate on a scale much smaller than the observed field features may explain the broad scale-independence of the observed drift rate. These advantages, along with those discussed above, lend credibility to the theory presented here—that hydrodynamic QG Rossby waves with radially-extended structures may underpin the westward drift present in geomagnetic secular variation records.

Data accessibility. This article has no additional data.

Competing interests. I declare I have no competing interests.

Funding. The author is funded by an EPSRC Doctoral Training Award. The majority of this work was completed during an academic visit to ETH Zürich, funded by a David Crighton fellowship from the Department of Applied Mathematics and Theoretical Physics, University of Cambridge, UK.

Acknowledgements. I am grateful to Andrew Jackson and the EPM group at ETH Zürich for hosting me for a two-month academic visit in autumn 2017. Helpful suggestion for improvements to this manuscript were provided by Jack Atkinson, Peter Davidson, Andrew Jackson, Ben McDermott and two anonymous reviewers.

## References

1. Halley E. 1692 An account of the cause of the change of the variation of the magnetical needle. with an hypothesis of the structure of the internal parts of the earth: as it was proposed to the Royal Society in one of their late meetings. *Phil. Trans.* **17**, 563–578. (doi:10.1098/rstl.1686.0107)
2. Bullard EC, Freeman C, Gellman H, Nixon J. 1950 The westward drift of the Earth's magnetic field. *Phil. Trans. R. Soc. Lond. A* **243**, 67–92. (doi:10.1098/rsta.1950.0014)
3. Jackson A, Finlay C. 2015 Geomagnetic secular variation and its applications to the core. In *Treatise on geophysics* (ed. G Schubert), pp. 137–184, 2nd edn. Oxford, UK: Elsevier.
4. Holme R, Olsen N, Bairstow FL. 2011 Mapping geomagnetic secular variation at the core–mantle boundary. *Geophys. J. Int.* **186**, 521–528. (doi:10.1111/j.1365-246X.2011.05066.x)
5. Finlay CC, Jackson A. 2003 Equatorially dominated magnetic field change at the surface of Earth's core. *Science* **300**, 2084–2086. (doi:10.1126/science.1083324)
6. Yukutake T. 1962 The westward drift of the magnetic field of the earth. *Bull. Earthquake Res. Inst.-Univ. Tokyo* **40**, 1–65.
7. Jault D, Gire C, LeMouel JL. 1988 Westward drift, core motions and exchanges of angular momentum between core and mantle. *Nature* **333**, 353–356. (doi:10.1038/333353a0)
8. Jackson A. 2003 Intense equatorial flux spots on the surface of the Earth's core. *Nature* **424**, 760–763. (doi:10.1038/nature01879)
9. Fisk HW. 1931 Isopors and isoporic movements. *Intern. Geodetical Geophys. Union, Sect. Terrest. Magnetism Elec. Stockholm Assembly 1930, Bull.* **8**, 280–292.
10. Roberts PH, King EM. 2013 On the genesis of the Earth's magnetism. *Rep. Prog. Phys.* **76**, 096801. (doi:10.1088/0034-4885/76/9/096801)
11. de Wijs GA, Kresse G, Vočadlo L, Dobson D, Alfè D, Gillan MJ, Price GD. 1998 The viscosity of liquid iron at the physical conditions of the Earth's core. *Nature* **392**, 805–807. (doi:10.1038/33905)
12. Proudman J. 1916 On the motion of solids in a liquid possessing vorticity. *Proc. R. Soc. Lond. A* **92**, 408–424. (doi:10.1098/rspa.1916.0026)
13. Taylor GI. 1917 Motion of solids in fluids when the flow is not irrotational. *Proc. R. Soc. Lond. A* **93**, 99–113. (doi:10.1098/rspa.1917.0007)
14. Pais MA, Jault D. 2008 Quasi-geostrophic flows responsible for the secular variation of the Earth's magnetic field. *Geophys. J. Int.* **173**, 421–443. (doi:10.1111/j.1365-246X.2008.03741.x)
15. Hide R. 1966 Free hydromagnetic oscillations of the Earth's core and the theory of the geomagnetic secular variation. *Proc. R. Soc. Lond. A* **259**, 615–647. (doi:10.1098/rsta.1966.0026)
16. Finlay CC, Dumberry M, Chulliat A, Pais MA. 2010 Short timescale core dynamics: theory and observations. *Space. Sci. Rev.* **155**, 177–218. (doi:10.1007/s11214-010-9691-6)
17. Hori K, Jones CA, Teed RJ. 2015 Slow magnetic Rossby waves in the Earth's core. *Geophys. Res. Lett.* **42**, 2015GL064733. (doi:10.1002/2015GL064733)

18. Hori K, Teed RJ, Jones CA. 2017 The dynamics of magnetic Rossby waves in spherical dynamo simulations: a signature of strong-field dynamos? *Phys. Earth Planet. Inter.* **276**, 66–85. (doi:10.1016/j.pepi.2017.07.008)
19. Cardin P, Olson P. 1994 Chaotic thermal convection in a rapidly rotating spherical shell: consequences for flow in the outer core. *Phys. Earth Planet. Inter.* **82**, 235–259. (doi:10.1016/0031-9201(94)90075-2)
20. Schaeffer N, Cardin P. 2005 Quasigeostrophic model of the instabilities of the Stewartson layer in flat and depth-varying containers. *Phys. Fluids* **17**, 104111. (doi:10.1063/1.2073547)
21. Canet E, Finlay CC, Fournier A. 2014 Hydromagnetic quasi-geostrophic modes in rapidly rotating planetary cores. *Phys. Earth Planet. Inter.* **229**, 1–15. (doi:10.1016/j.pepi.2013.12.006)
22. Aubert J, Gillet N, Cardin P. 2003 Quasigeostrophic models of convection in rotating spherical shells. *Geochem. Geophys. Geosyst.* **4**, 1052. (doi:10.1029/2002GC000456)
23. Gillet N, Jones CA. 2006 The quasi-geostrophic model for rapidly rotating spherical convection outside the tangent cylinder. *J. Fluid. Mech.* **554**, 343–369. (doi:10.1017/S0022112006009219)
24. Guervilly C, Cardin P. 2016 Subcritical convection of liquid metals in a rotating sphere using a quasi-geostrophic model. *J. Fluid. Mech.* **808**, 61–89. (doi:10.1017/jfm.2016.631)
25. Maffei S, Jackson A, Livermore PW. 2017 Characterization of columnar inertial modes in rapidly rotating spheres and spheroids. *Proc. R. Soc. A* **473**, 20170181. (doi:10.1098/rspa.2017.0181)
26. Jault D. 2008 Axial invariance of rapidly varying diffusionless motions in the Earth's core interior. *Phys. Earth Planet. Inter.* **166**, 67–76. (doi:10.1016/j.pepi.2007.11.001)
27. Labbé F, Jault D, Gillet N. 2015 On magnetostrophic inertia-less waves in quasi-geostrophic models of planetary cores. *Geophys. Astrophys. Fluid Dyn.* **109**, 587–610. (doi:10.1080/03091929.2015.1094569)
28. Zhang K, Earnshaw P, Liao X, Busse FH. 2001 On inertial waves in a rotating fluid sphere. *J. Fluid. Mech.* **437**, 103–119. (doi:10.1017/S0022112001004049)
29. Davidson PA. 2013 *Turbulence in rotating, stratified and electrically conducting fluids*. Cambridge, UK: Cambridge University Press.
30. Vallis GK. 2017 *Atmospheric and oceanic fluid dynamics: fundamentals and large-scale circulation*, 2nd edn. Cambridge, UK: Cambridge University Press.
31. Jault D, Finlay C. 2015 Waves in the core and mechanical core–mantle interactions. In *Treatise on geophysics* (ed. G Schubert), vol. 8, pp. 225–245. Amsterdam, The Netherlands: Elsevier Science.
32. Duba CT, McKenzie JF. 2012 Propagation properties of Rossby waves for latitudinal $\beta$-plane variations of $f$ and zonal variations of the shallow water speed. *Ann. Geophys.* **30**, 849–855. (doi:10.5194/angeo-30-849-2012)
33. Davidson PA, Staplehurst PJ, Dalziel SB. 2006 On the evolution of eddies in a rapidly rotating system. *J. Fluid. Mech.* **557**, 135–144. (doi:10.1017/S0022112006009827)
34. Schaeffer N, Jault D, Nataf HC, Fournier A. 2017 Turbulent geodynamo simulations: a leap towards Earth's core. *Geophys. J. Int.* **211**, 1–29. (doi:10.1093/gji/ggx265)
35. Olson P. 2011 Laboratory experiments on the dynamics of the core. *Phys. Earth Planet. Inter.* **187**, 139–156. (doi:10.1016/j.pepi.2011.08.006)
36. Gillet N, Schaeffer N, Jault D. 2012 Rationale and geophysical evidence for quasi-geostrophic rapid dynamics within the Earth's outer core. *Phys. Earth Planet. Inter.* **202–203**, 78–88. (doi:10.1016/j.pepi.2012.03.006)
37. Abramowitz M, Stegun IA. 1964 *Handbook of mathematical functions: with formulas, graphs, and mathematical tables*. Chelmsford, MA: Courier Corporation.
38. Davidson PA. 2016 Dynamos driven by helical waves: scaling laws for numerical dynamos and for the planets. *Geophys. J. Int.* **207**, 680–690. (doi:10.1093/gji/ggw297)
39. Roberts PH, Scott S. 1965 On analysis of the secular variation. *J. Geomagn. Geoelectr.* **17**, 137–151. (doi:10.5636/jgg.17.137)
40. Finlay C. 2005 Hydromagnetic waves in Earth's core and their influence on geomagnetic secular variation. PhD thesis, University of Leeds, Leeds, UK.
41. Aubert J, Finlay CC, Fournier A. 2013 Bottom-up control of geomagnetic secular variation by the Earth's inner core. *Nature* **502**, 219–223. (doi:10.1038/nature12574)
42. Hide R, Roberts PH. 1979 How strong is the magnetic field in the Earth's liquid core? *Phys. Earth Planet. Inter* **20**, 124–126. (doi:10.1016/0031-9201(79)90034-7)